Thermal Infrared (3–14μm) Bidirectional Reflectance Measurements of Sands and Soils

William C. Snyder, Zhengming Wan, Yulin Zhang, and Yue-Zhong Feng

6832 Ellison Hall

Institute for Computational Earth System Science

University of California

Santa Barbara, CA 93106

submitted April 23, 1996, revised July 19, 1996

Phone: (805) 893-7353

ABSTRACT

Recent day/night land surface temperature (LST) algorithms can recover both emissivity and temperature, but require some assumptions about the relative optical properties of natural materials in the thermal infrared. We constructed a goniometer and measured the spectral, angular emissivity and bidirectional reflectance of sands and soils in the 3-14 μm range. In this paper we present the results for five diverse surfaces and examine the validity of the LST assumptions. We conclude that the change in emissivity with angle was small across the entire range for all of the materials except sand. In addition, for all of the materials, the measured variation in bidirectional reflectance anisotropy with wavelength was small enough to neglect.

I. Introduction

The optical properties of sands and soils in the thermal infrared (3 to 14μm) are needed for the remote sensing of surface temperature (Wan and Dozier, 1989) and in models of surface energy budget (Norman et al., 1995). A fundamental optical characterization of a diffuse material is its spectral, bidirectional reflectance distribution function (BRDF) at all incident and reflected angles. The integrated BRDF provides physical quantities such as angular, directional-hemispherical reflectance, and from Kirchhoff's law, the angular emissivity. Measurement of spectral BRDF in the thermal bands, however, is problematic. Previous studies in the thermal infrared have measured spectral and angular reflectance of sands and soils (Labed and Stoll, 1991), near-nadir spectral reflectance (Salisbury and D'Aria, 1992b; Salisbury and D'Aria, 1994), and non-spectral bidirectional reflectance (Becker et al., 1985). For the present study we designed and constructed a goniometer that provides high-resolution spectral BRDF from 3 to 14 μm (Snyder and Wan, 1996). These measurements were made to support improved land surface temperature (LST) algorithms for the NASA MODIS satellite instrument (Solomonson et al., 1989). In particular, proposed day/night LST methods for NOAA AVHRR and MODIS (Li and Becker, 1993; Wan and Li, 1996) require some assumptions about the BRDF anisotropy that have not been verified. These day/night LST methods are valuable because they can recover both temperature and emissivity.

Most satellite sea and land surface temperature algorithms are based on variations of the split-window method, that applies the radiance in two or more thermal bands of a multi-spectral sensor to eliminate the atmospheric effects and extract the surface radiance. There are many recent improvements to split window methods for LST (Kerr et al., 1992;

Prata, 1994; Wan and Dozier, 1996). All such methods require accurate knowledge of the surface emissivity to convert the radiance to surface temperature. Better than 0.3K accuracy is possible for water because of the uniformity and predictability of the surface properties. Over land, the errors in emissivity significantly reduce the temperature accuracy. Specifically, over vegetation, the split-window accuracy is about 1.0K, but is considerably worse over bare soils (Kerr et al., 1992). Errors in emissivity are small for medium to dense vegetation canopies because multiple scattering and the relatively low component reflectance cause the overall emissivity to approach unity. In semi-arid and arid regions for which the viewed component of sand or soil increases, the accuracy of the estimated emissivity will be poorer. For these surfaces there is strong variability in emissivity caused by subtle changes in material composition and surface properties.

Because of this it will be difficult to achieve the MODIS LST error goal of 1.0 K over bare soils. This accuracy would require a comprehensive database of soil emissivities and an accurate land cover classification with high spatial and class resolution. The classification would also need to include temporal meteorological changes that affect surface moisture because this changes the emissivity (Salisbury and D'Aria, 1992a). Neither a complete database nor the classification are available. Consequently, there has been much effort devoted to alternative LST methods which can recover temperature without *a priori* knowledge of the emissivity.

Surface temperature from one multiband measurement is well known to be an underdetermined problem, even if atmospheric effects can be corrected by the use of independent measurement data. Success has been reported in recovering relative emissivity spectra for

mineralogical classification, etc., (Becker and Li, 1990). The extension of relative spectra to absolute emissivity and temperature is made possible by assuming at least one emissivity-related absolute value (Khale and Alley, 1992; Kealy and Hook, 1993). On the other hand, for the same surface measured at two temperatures, say, in day and night, both the daytime and nighttime temperatures and the band-averaged emissivities can be recovered. For the total number of variables to be reduced, the day-night algorithms still must make some assumptions about the band-to-band relation of the normalized BRDF of the surface. Because these involve relative properties, however, they will hold over a wider range of actual conditions. In this article we will present measurements of some sands and soils and evaluate the validity of these assumptions.

II. LST Algorithm Requirements

With a single, n-band measurement we have n observations and n unknown emissivities. There is also the unknown surface temperature and additional atmospheric unknowns that are required to find the upwelling atmospheric radiance, the downwelling irradiance, and the atmospheric transmissions. In contrast, with daytime and nighttime measurements there will be a large surface temperature difference but constant emissivities, and we have $2n$ observations, so in principle we can solve for the two temperatures, the n emissivities, and an additional $2n - (n + 2)$ unknowns (Watson, 1992). The proposed MODIS day/night LST algorithm uses the seven bands shown in Table 1.

Because the reflected thermal and scattered solar downwelling irradiances are small with respect to the surface thermal radiance, we can link them to the downwelling irradiance with

the surface reflectance by the use of the Lambertian approximation. The radiance at the detector, L_i, for a particular geometry and spectral band, i, is then:

$$L_i = t_1(i)\varepsilon_i B_i(T_s) + t_2(i)(1-\varepsilon_i)\frac{E_d(i)}{\pi} + t_3(i)f_i E_s(i) + L_u(i). \tag{1}$$

All terms are band-averaged quantities including the Planck radiance, $B(T_s)$. Here, T_s is the surface temperature, ε_i is emissivity and f_i is the BRDF of the surface. With the day and night atmospheric temperatures and column water vapors we can apply atmospheric models to predict the band averaged transmissions weighted by the in-band spectral properties of each term, $t_1(i), t_2(i)$, and $t_3(i)$. Similarly, we can find the thermal and scattered solar downwelling irradiance, $E_d(i)$, the direct solar irradiance, $E_s(i)$, and the atmospheric upwelling radiance, $L_u(i)$. The direct solar term is non-zero only for the three mid-infrared bands (bands 20, 22, and 23) during daytime measurements, so three of the seven daytime equations require BRDF values. For a given geometry, we would like to reduce these three BRDF values to one non-spectral factor that is scaled by the spectral band reflectance (already related implicitly to emissivity).

Therefore, if we define this anisotropy factor as:

$$\alpha = \frac{\pi f}{(1-\varepsilon)}, \tag{2}$$

and assume it is independent of the band, i, Equation (1) becomes:

$$L_i = t_1(i)\varepsilon_i B_i(T_s) + \frac{(1-\varepsilon_i)}{\pi}\left[t_2(i)E_d(i) + \alpha t_3(i)E_s(i)\right] + L_u(i). \tag{3}$$

The seven MODIS LST bands will give seven equations for the day and seven for the night. The unknowns are the seven emissivities, one non-spectral anisotropy value, and the day and night surface temperatures. Simulations are applied to find the remaining unknowns from

the day and night column water vapors and air temperature parameters. Therefore, there are a total of 14 equations and 14 unknowns. Least-squares fitting methods may be applied to solve for the desired variables. Our simulations in wide ranges of surface emissivities and atmospheric conditions have shown that we can recover accurate surface temperatures if the following assumptions hold. Details of this day/night algorithm may be found in Wan and Li (1996).

We have assumed that there is one surface emissivity for each band and a single temperature within a given pixel for each measurement. For mixed pixels, the recovered emissivities will be averaged values and the recovered temperature will be the value from averaged radiance. In addition, although surface emissivity may vary with different view angles and changes in the surface properties between the day and night measurements, we have assumed that the variations are small. Finally, we have assumed that the anisotropy variations among the mid-infrared MODIS bands is small. We will show by theory and measurements that the angular change in emissivity can usually be neglected, and that the three mid-infrared BRDF values can be reduced to one constant non-spectral anisotropy scaled by the spectral reflectance.

III. Model Estimates

There are several effects that could change the anisotropy with wavelength. For wavelengths near the soil particle size, the scattering physics lies in the range commonly called the resonance region, in which the complete wave nature of the incident radiation must be considered in the solution of scattering phase functions (Barber and Yeh, 1975). The change

in anisotropy caused by scattering physics is difficult to model because natural soil particles are rough, not spherical, and have a range of sizes. Therefore, for our approximation, we will consider only the effects of a change of the particle single-scattering reflectance with wavelength. As the single-scattering reflectance changes, the portion of the phase function caused by multiple scattering will change nonlinearly. This will change the normalized shape of the BRDF. One model that accounts for such multiple scattering is a particulate model originally developed for extraterrestrial studies (Hapke, 1981) and subsequently applied to terrestrial sands and soils in the visible and near infrared (Pinty, 1989; Ahmad, 1992; Jacquemond, 1992). Follow-on work improves this model (Liang, 1996), but we apply a simpler form here to estimate the variation in anisotropy with reflectance and the variation in emissivity with view angle.

Following Pinty (1989), the BRDF model is:

$$f = \frac{\rho_0}{4\pi} \frac{1}{\cos\theta_i + \cos\theta_r} \left([1 + B(\xi)]\, P(\xi) + H(\theta_i, \rho_0) H(\theta_r, \rho_0) - 1 \right), \tag{4}$$

Here, θ_i, θ_r are the incident and reflected zenith angles respectively, and ρ_0 is the single-scattering reflectance of the component particles. The scattering angle at a relative azimuth, ϕ, is:

$$\xi = \arccos(\cos\theta_i \cos\theta_r + \sin\theta_i \sin\theta_r \cos\phi). \tag{5}$$

The phase function $P(\xi)$ is approximated by a polynomial with empirical parameters, b, and c:

$$P(\xi) = 1 + b\cos\xi + c\frac{3\cos^2\xi - 1}{2}. \tag{6}$$

The backscattering function is:

$$B(\xi) = \frac{S(0)}{\rho_0 P(0)} \frac{1}{1 + (1/h)\tan(\xi/2)}, \tag{7}$$

where $S(0)$ is a parameter. Finally the $H(\xi)$ functions in the multiple-scattering term are approximated by:

$$H(\theta, \rho_0) = \frac{1 + 2\cos\theta}{1 + 2\cos\theta\sqrt{1 - \rho_0}}. \tag{8}$$

Based on our measured data, we chose a set of round numbers that represented a range of materials over a range of wavelengths: $h = 0.1$, $S(0) = 1.0$, $b = 0.5$, and $c = 0$. Use of these approximate values is acceptable because we only wish to estimate relative variations. The model was evaluated with the single-scattering reflectance set to $\rho_0 = 0.3$ and then changed to $\rho_0 = 0.2$. This corresponds to the largest spectral change in surface reflectance we have measured among the MODIS bands 20, 22, and 23. Numerically integrating the results for both settings gave the directional-hemispherical reflectance, which was then used to normalize the BRDF to give the anisotropy.

Figure 1 shows a section of the modeled anisotropy curve in the 30-degree azimuth plane with an incident angle of 32 degrees (0.55 radians on the positive zenith axis). Clearly the difference between the two curves for $\rho_0 = 0.3$ and $\rho_0 = 0.2$ is small with respect to the overall variation. We evaluated the anisotropy variation over a realistic range of azimuth, and incident and reflected zenith angles. The RMS variation over the range was 4.8% and the maximum error was 9.5%. Because we used a large reflectance change, these values should be considered upper bounds for typical materials.

The same model provided the relative change in emissivity with view angle. For the 3-5 μm region, we set $\rho_0 = 0.3$, the ratio of the emissivity at 53 degrees view zenith to that at 10 degrees was 0.986. For the 8-14 μm region we set $\rho_0 = 0.1$, and the ratio was 0.996. These ratios are stronger functions of the chosen parameters than the anisotropy change

and therefore are less reliable estimates. These modeled values support the LST algorithm assumptions of small spectral dependence in anisotropy and small angular dependence in emissivity.

IV. Measurements

Measurements of spectral reflectance in the thermal region are difficult because natural materials often have a very low reflectance. Active reflectance measurement requires a source, and a wideband source both illuminates and heats the sample, causing a radiance change that is a combination of the surface reflection and thermal emission. In previous studies, one system measured the wideband thermal infrared BRDF by detecting the radiance change from modulating a wideband infrared source based on a heated SiC element (Becker et al., 1981; Becker et al., 1985). A 10.6 μm CO_2 laser was also used as a narrowband source. The modulation method reduces the effects of surface heating and cancels the unchanging background contribution. Other systems applied the emissive technique with a heated sample to measure spectral emissivity at nadir with the box method (Nerry et al., 1990) and to characterize the dependence of spectral emissivity on angle with a mirror system (Labed and Stoll, 1991). All of these instruments were employed to study soil and sand properties. With our spectral infrared bidirectional reflectance and emissivity (SIBRE) instrument, the thermal infrared source is a heated ceramic plate, and we measure reflected radiance with a Fourier transform spectrometer that responds in the 3-14 μm range. Both of these are mounted on a pointing system that affords a wide range of geometrical combinations over the sample hemisphere. Because of the practical aspects of Fourier scanning, we use slow-speed

source chopping to eliminate the background radiance and instrument offsets. The surface temperature change caused by the source is significant, and is corrected by curve-fitting the detected radiance for each source state (Snyder and Wan, 1996). A four-step differential-ratio method is used to cancel the background, instrument calibration, and source temperature terms. Our system is unique because it measures hyperspectral BRDF across the thermal infrared over a wide range of source and detector angles. Moreover, it can measure rougher surfaces because it has a larger spot size ($\sim$5 cm diameter) than integrating sphere systems ($<$ 1 cm). The resulting measurements may be integrated over angle or wavelength to give surface properties tailored for a specific satellite sensor.

True BRDF is a differential quantity, but if it is smooth it can be approximated with bidirectional reflectance measurements. The SIBRE spectrometer measures the reflected radiance inside a solid angle of approximately one milli-steradian. The source produces wideband infrared irradiance on the surface from a solid angle of 43 milli-steradians. Figure 2 shows the source zeniths and relative azimuths, and the set of five detector zenith angles that are repeated for each source position. The source zenith angle ranges from 2 to 70 degrees, the detector angle ranges from 10 to 53 degrees. The relative azimuth ranges from 30 to 180 degrees with a step size that depends on the source zenith. The total number of combinations is 187, but we also measure diffuse materials with a subset of 45 geometries. We have characterized several diffuse materials with both 45 and 187 geometrical combinations and obtained almost the same results. At each geometry we record spectra sampled at 2 cm^{-1} intervals over a useful range of 700 to 2800 cm^{-1}.

Further details of the SIBRE instrument and the recovery of BRDF from radiance mea-

surements are given by Snyder and Wan (1996). The BRDF spectra for each material are filtered with a 7-bin median and 7-bin moving average. The averaged data are also filtered spatially by the weighting kernel $k = \cos^n(\cdot)$ for both the incident and reflected directions. Here, k is zero when the argument is larger than $\pi/2$ and we determined that for the subset of 45 geometries, a value of $n = 11$ filters the sampling but preserves the salient features of the BRDF. Moreover, Hemholtz reciprocity (Nicodemus, 1967) is imposed on the BRDF by averaging the two reconstructed values that result from switching the incident and reflected zenith angles at the same relative azimuth. What we report is thus the true BRDF filtered by convolution with the finite source and detector angles, and by convolution with the reconstruction kernel.

We checked our BRDF values by measuring reflectance with an integrating sphere over the same spectral range. These measurements are compared with the integrated BRDF from the SIBRE. For the integrating sphere, we apply a four-step differential-ratio method based on a calibrated, sintered gold standard reference. Measurements of water on the integrating sphere exhibit systematic reflectance errors of less than 0.002 across the spectrum when compared to Fresnel theory. Water has a low reflectance: approximately 0.01-0.03 in the 3-14 μm range. The integrating sphere was then used as a reference to check the bias in the SIBRE measurements. For the low-reflectance materials near 800 cm^{-1}, the mean difference between the integrating sphere and the SIBRE reflectance was 0.005. For the higher reflectance regions near 2500 cm^{-1} the mean difference was 0.02. The standard deviation of the differences was 0.003 and 0.012 respectively. These errors include not only the error in instrument calibration, but also errors caused by temporal variations in the illumination

and hemispherical response weighting. It should be noted that there are differences in the response of the instruments to a backscattering lobe, which commonly occurs with natural materials. Finally it should be noted that the bias errors tend to cancel in the computations of the relative quantities of interest here.

Spectral BRDF measurements of 15 sands and soils with different compositions and surface textures produced a wide range of reflectances and anisotropies. The five materials presented here represent the extremes and are summarized in Table 2. The organic soil is decomposing soil litter that was very dark brown with a coarse surface. It was air dried only, and remained somewhat moist during measurements. The sand is beach sand that was screened, washed in distilled water, and air dried. Next is a sample of screened silt loam soil from Lincoln county, Kentucky. Although not technically so, we will call this "silt." This had a few dry grass pieces and was reported to have 3% carbon content with various other minerals. It was one of nine obtained from National Soil Survey Center in Lincoln, Nebraska. After processing, screening, and drying, the Soil Survey Center samples are archived primarily for composition studies. For a more volumetric surface, we placed pieces of green grass and dry leaves over a sample of the organic soil so that it was approximately 40% covered. Finally, the gravel sample is a light tan mollisol from a grassy area in Santa Barbara, California. This material had a large range of particle sizes, but we eliminated the sand and silt in this sample smaller than 2mm by screening. The remaining gravel included some organic content and dust.

V. Results and Discussion

The BRDF measurements of the materials were numerically integrated to provide the spectral directional-hemispherical reflectances that are presented in Figure 3. These curves correspond to a 10-degree view angle. The seven reference lines correspond to the seven MODIS band centers. Note that from approximately 1300 cm^{-1} to 1900 cm^{-1} and in a small region around 2350 cm^{-1} there is strong atmospheric attenuation. The measurements in these regions are less accurate because the SIBRE has a path length of $\sim$ 3 m. In the thermal infrared, the reflectance variability depends strongly on the organic content, with the sand having the highest peaks and the organic soil having the lowest. Complete descriptions of the reflectance features for many materials are available (Salisbury and D'Aria, 1992a; Salisbury and D'Aria, 1992b; Salisbury and D'Aria, 1994). Figure 4 shows the 8-14 μm region with the ordinate changed to emissivity. The set of five dissimilar samples of sands and soils exhibit a uniformly high emissivity for wavelengths longer than 10.5 μm (0.96 – 0.995). This agrees with the box method measurements by Nerry et al. (1990). Even without the sand sample, however, emissivity variations in the 8-14 μm region bands exceed 0.01.

To validate our assumptions for LST algorithms, we examined the spectral, angular change of the five emissivities. The difference between the day and night look angles for one or several MODIS instruments can exceed 60 degrees, but this extreme is unlikely. Figure 5 shows the ratio of the emissivity at 53 degrees to that at 10 degrees for the five materials. The four soil materials change less than one percent across the spectrum. Sand showed larger variations, which compare closely with those from previous angular emissivity studies (Labed and Stoll, 1991). In the case of bare sand, the emissivity variations with angle may

not be small enough to neglect for LST applications.

Next, we compare the anisotropies of the materials. Figure 6 shows these in the same geometry that was used in the model estimate. The values are band-averaged at 4.06 μm (2460 cm^{-1}) corresponding to MODIS band 23. The soils exhibit backscattering peaks of various magnitudes as expected from models and measurements in the near infrared and visible (Ahmad and Deering, 1992; Roujean et al., 1992). The soil and vegetation mix displays a volumetric scattering characteristic as predicted by Roujean et al. (1992) with a minimum near nadir and larger values at extreme angles. Sand has a small amount of back and forward scattering and is the most isotropic of the materials, as was determined by Becker et al. (1985) in the 8-14μm range. Note that if we did not account for the anisotropy in the LST algorithm and instead used the reflectance with the Lambertian assumption, the error in the reflected direct solar term would be higher than 10% for some of the materials.

Figures 7 through 11 show these anisotropy curves at each of the three MODIS bands of interest. Ideally, there would be no differences among the curves for a given material. It is clear that the anisotropy is different for different materials, but stays quite constant across the 3.5-4.2 μm range for each of the five samples. As was done for the model, we computed RMS and maximum variation for the 45 measured geometries between the band 23 anisotropy values and those for bands 22 and 20. The results are summarized in Table 3. The RMS variations are approximately 1-3% and the maximum variations are 2-7%.

VI. Summary and Conclusions

The measurements presented in this paper further the knowledge of the optical properties of terrestrial materials in the thermal infrared. The results support some assumptions required for recent day/night LST algorithms. In particular, we determined that the change in emissivity between 10 and 53 degrees was small: less than 1% for all materials tested except sand. From simulations we have concluded that a change of this size is acceptable in the seven-band day/night LST algorithm. For bare sand, the change ranged up to 4% in the 8-10 μm region and was approximately 2% in the 3-5 μm and 10-14 μm regions. Consequently, angular emissivity effects need to be considered to achieve high LST accuracies with sand.

In addition, we examined the BRDF of the samples in the 3–5 μm range where the reflected solar irradiance is significant. The BRDF exhibits the same characteristics that appear in other studies of these materials. Our model estimates indicated only a small change in BRDF anisotropy with wavelength. We confirmed by measurements that variation in the anisotropy was 1-2% RMS among the MODIS bands 20, 22, and 23. This is low enough to assume it is constant for the proposed day/night LST algorithm.

Ideal samples would be unprocessed, undisturbed sections of natural surfaces. This would preserve the structure and weathering that can affect optical properties. Of course, such samples are more difficult to collect and measure. Although they are processed, we feel that the samples we used demonstrate the salient properties of natural surfaces. This is true particularly for the bare surfaces where the day/night approach is most useful. For future work concerning absolute optical properties, we plan to collect and measure unprocessed samples.

VII. Acknowledgments

This work was supported by Earth Observing System Program contract NAS5-31370 of the National Aeronautics and Space Administration. We would also like to thank the reviewers for helpful comments.

References

Ahmad, S.P., and Deering, D.W. (1992), A simple analytical function for bidirectional reflectance, *J. Geophys. Res.* 97:18,867-18,886.

Barber, P. and Yeh, C. (1975), Scattering of electromagnetic waves by arbitrarily shaped dielectric bodies, *Appl. Optics* 14:2864-2872.

Becker, F., Ngai, W., and Stoll, M.P. (1981), An active method for measuring thermal emissivities: Implications and perspectives for remote sensing, *Adv. Space Res.* 1:193-210.

Becker, F., Ramanantsizehena, P., and Stoll, M.P. (1985), Angular variation of the bidirectional reflectance of bare soils in the thermal infrared, *Appl. Optics* 24:365-375.

Becker, F., and Li, Z. (1990), Temperature-independent spectral indices in the thermal infrared bands, *Remote Sens. Environ.* 32:17-33.

Hapke, B. (1981), Bidirectional Reflectance Spectroscopy 1. Theory, *J. Geophys. Res.* 86:3039-3054

Jacquemoud, S., Baret, F., and Hanocq, J.F. (1992), Modeling spectral and bidirectional soil reflectance, *Remote Sens. Environ.* 41:123-132.

Kahle, A.B. and Alley, R.E. (1992), Separation of temperature and emittance in remotely sensed radiance measurements, *Remote Sens. Environ.* 42:107-111.

Kealy, P.S., and Hook, S.J. (1993), Separating temperature and emissivity in thermal infrared multispectral scanner data: implications for recovering land surface temperatures, *IEEE Trans. Geosci. Remote Sens.* 31:1155-1164.

Kerr, Y.H., Lagouarde, J.P., Imbernon, J. (1992), Accurate land surface temperature retrieval from AVHRR data with use of an improved split window algorithm, *Remote Sens. Environ.* 41:197:209.

Labed, J. and Stoll, M. (1991), Angular variation of land surface spectral emissivity in the thermal infrared: laboratory investigations on bare soils, *Int. J. Remote Sens.* 12:2299-2310.

Li, Z., and Becker, F. (1993), Feasibility of land surface temperature and emissivity determination from AVHRR data, *Remote Sens. Environ.* 43:67-85.

Liang, S. and Townshend, J.R.G. (1996), A modified Hapke model for soil bidirectional reflectance, *Remote Sens. Environ.* 55:1-10.

Nerry, F., Labed, J., and Stoll, M.P. (1990), Spectral properties of land surfaces in the thermal infrared 1. Laboratory measurements of absolute spectral emissivity signatures, *J. Geophys. Res.* 95:7027-7044.

Nicodemus, F.E. (1967), In *Applied Optics and Optical Engineering* (R. Kingslake, Ed.), Academic Press, New York, Chap. 8 in Volume IV.

Norman, J.M., Divakarla, M., and Goel, N.S. (1995), Algorithms for extracting information from remote thermal-IR observations of the Earth's surface, *Remote Sens. Environ.* 51:157-168.

Pinty, B., Verstraete, M.M., and Dickinson, R.E. (1989), A physical model for predicting bidirectional reflectances over bare soil, *Remote Sens. Environ.* 27:273-288.

Prata, A.J. (1994), Land surface temperatures derived from the advanced very high resolution radiometer and the along-track scanning radiometer 2. experimental results and validation of AVHRR algorithms, *J. Geophys. Res.* 99:13025-13058.

Roujean, J., Leroy, M., and Dechamps, P. (1992), A bidirectional reflectance model of the Earth's surface for correction of remote sensing data, *J. Geophys. Res.* 97:20,455-20,468.

Salisbury, J.W. and D'Aria, D.M. (1992a), Infrared (8-14 μm) remote sensing of soil particle size, *Remote Sens. Environ.* 42:157-165.

Salisbury, J.W. and D'Aria, D.M. (1992b), Emissivity of terrestrial materials in the 8-14 μm atmospheric window, *Remote Sens. Environ.* 42:83-106.

Salisbury, J.W. and D'Aria, D.M. (1994), Emissivity of terrestrial materials in the 3-5 μm atmospheric window, *Remote Sens. Environ.* 47:345-361.

Snyder, W.C. and Wan, Z. (1996), Surface temperature correction for active infrared reflectance measurements of natural materials, *Appl. Optics* 35:2216-2220.

Salomonson, V., Barnes, W., Maymon, P., Montgomery, H., and Ostrow, H. (1989), MODIS: advanced facility instrument for studies of the Earth as a system, *IEEE Trans. Geosci. Remote Sens.* 27:145-153.

Wan, Z. and Dozier, J. (1989), Land-surface temperature measurement from space: physical principles and inverse modeling, *IEEE Trans. Geosci. Remote Sens.* 27:268-277.

Wan, Z. and Dozier, J. (1996), A generalized split-window algorithm for retrieving land-surface temperature measurement from space, *IEEE Trans. Geosci. Remote Sens.* 34:1-14 (in press).

Wan, Z. and Li, Z. (1996), A physics-based algorithm for retrieving land-surface emissivity and temperature from EOS/MODIS data, *IEEE Trans. Geosci. Remote Sens.* (revised).

Watson, K. (1992), Two-temperature method for measuring emissivity, *Remote Sens. Environ.* 42:117-121.

Table 1. MODIS Thermal Infrared Bands for LST

Band No.	**Spectral Range (μm)**
20	3.66–3.84
22	3.93–3.99
23	4.02–4.08
29	8.4–8.7
31	10.8–11.3
32	11.8–12.3
33	13.2–13.5

Table 2. Descriptions of the Five Sample Materials

Name	**Description & Texture**
ORG_SOIL	organic compost (0.03–6 mm)
SAND	washed sand (0.3–1.0 mm)
SILT	screened soil (0.01–0.3 mm)
VEG_SOIL	compost with grass and leaves
GRAVEL	gravel (2–10 mm)

Table 3. Percent Anisotropy Change for Bands 22 and 20 Relative to Band 23

Sample	**Band 22**		**Band 20**	
	RMS	**MAX**	**RMS**	**MAX**
ORG_SOIL	1.3	2.7	2.1	5.7
SAND	0.8	2.4	1.1	3.4
SILT	2.5	5.1	2.7	5.9
VEG_SOIL	1.5	2.9	3.3	6.8
GRAVEL	0.6	1.9	1.1	3.3
Average	1.3 %	3.0 %	2.1 %	5.0 %

List of Figures

1. Anisotropy change resulting from changing the single-scattering reflectance from 0.3 to 0.2 in the Hapke model. The plot is in the 30-degree azimuth plane with the angle of incidence at 32 degrees. Positive zenith values represent backscattering.

2. The detector declinations (triangles) and source positions (circles) for the BRDF measurements. The radial axis is linear in the zenith angle.

3. Spectral reflectance of the five sands and soils. Also shown are the center values of the MODIS bands of interest for land surface temperature.

4. Spectral emissivities of the five materials in the thermal infrared. The scale is set to show the variations in the four higher-emissivity materials in MODIS bands 31, 32, and 33.

5. Ratios of the angular emissivity at a 53-degree view angle to that at a 10-degree view angle.

6. Anisotropy of the five materials for MODIS band 23 in the 30-degree azimuth plane. The angle of incidence is 32 degrees. Positive zenith angles represent the backscatter direction.

7. Anisotropy of the organic soil in each of the three MODIS bands. The geometries are the same as for Figure 6.

8. Anisotropy variation for sand.

9. Anisotropy variation for silt.

10. Anisotropy variation for the soil/vegetation mix.

11. Anisotropy variation for gravel.

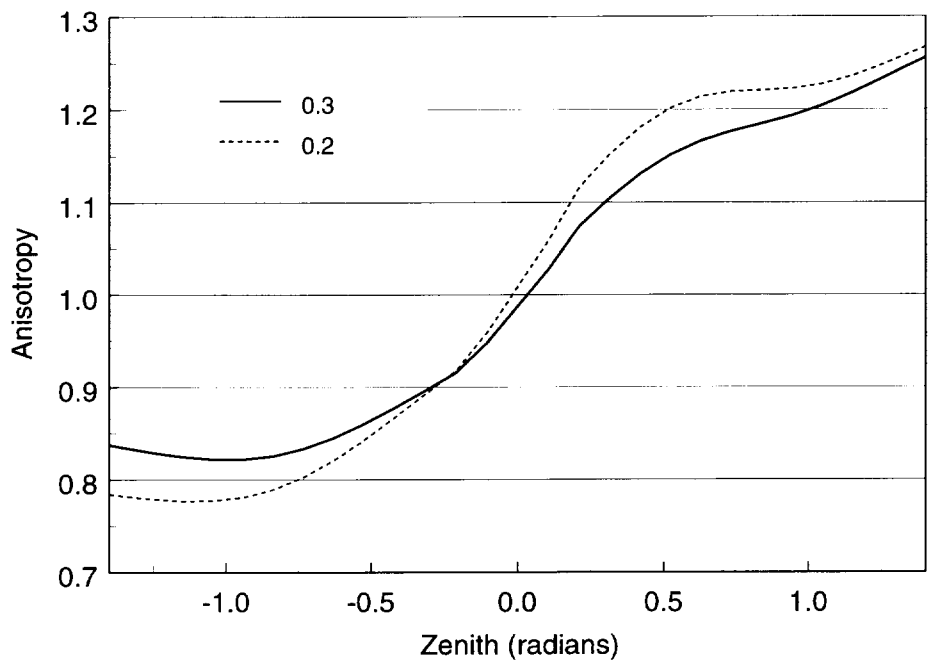

Figure 1: Anisotropy change resulting from changing the single-scattering reflectance from 0.3 to 0.2 in the Hapke model. The plot is in the 30-degree azimuth plane with the angle of incidence at 32 degrees. Positive zenith values represent backscattering.

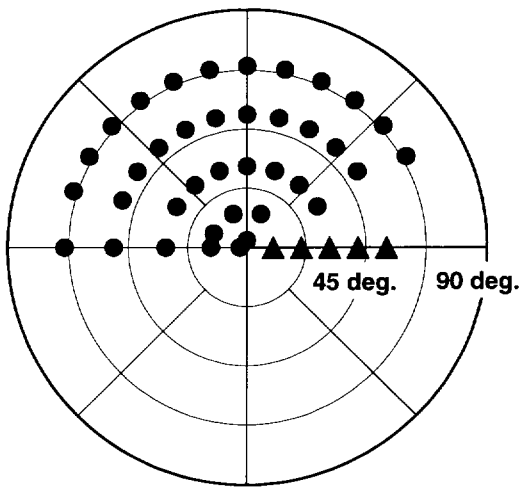

Figure 2: The detector declinations (triangles) and source positions (circles) for the BRDF measurements. The radial axis is linear in the zenith angle.

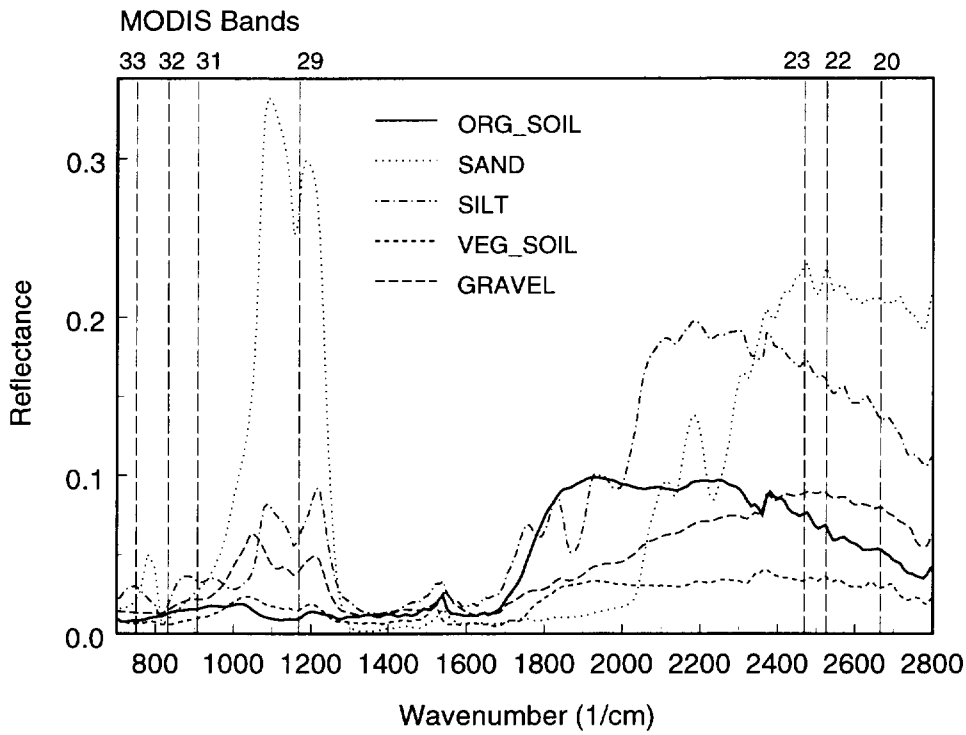

Figure 3: Spectral reflectance of the five sample materials. Also shown are the center values of the MODIS bands of interest for land surface temperature.

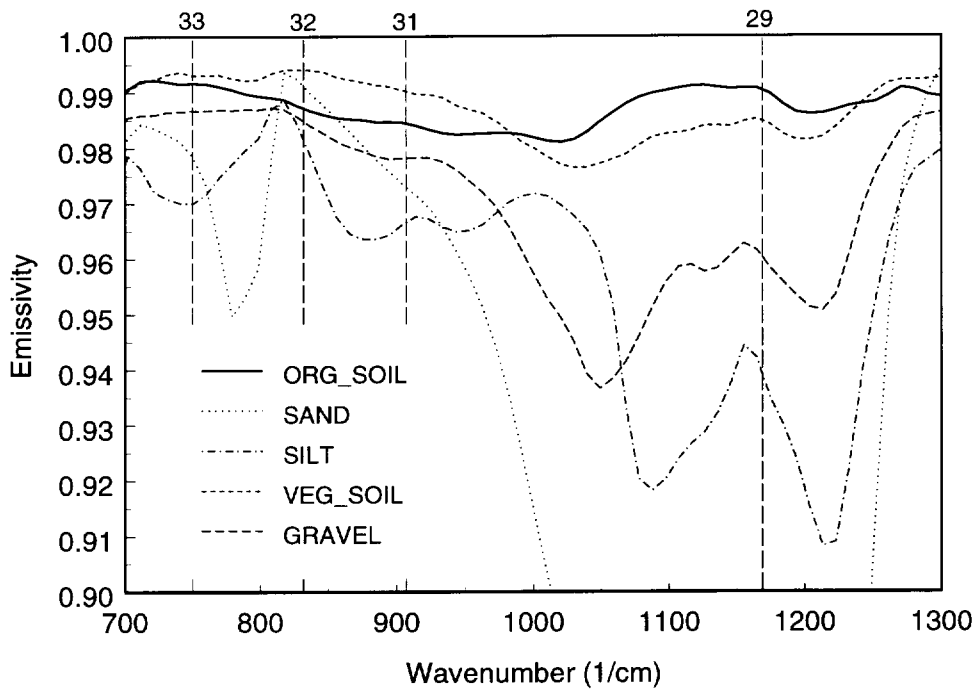

Figure 4: Spectral emissivities of the five materials in the thermal infrared. The scale is set to show the variations in the four higher-emissivity materials in MODIS bands 31, 32, and 33.

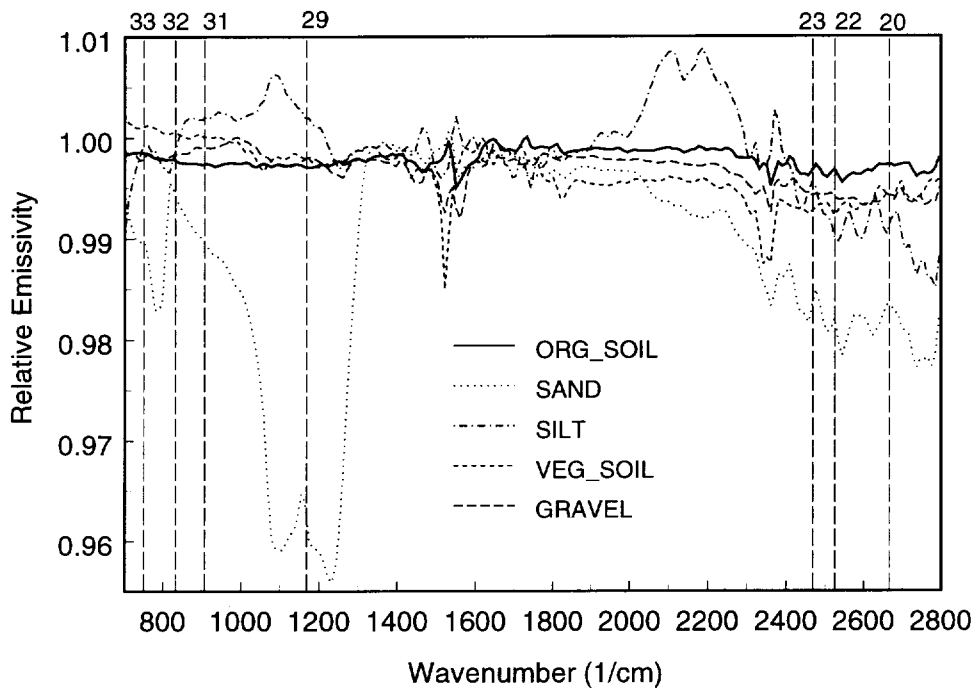

Figure 5: Ratios of the angular emissivity at a 53-degree view angle to that at a 10-degree view angle.

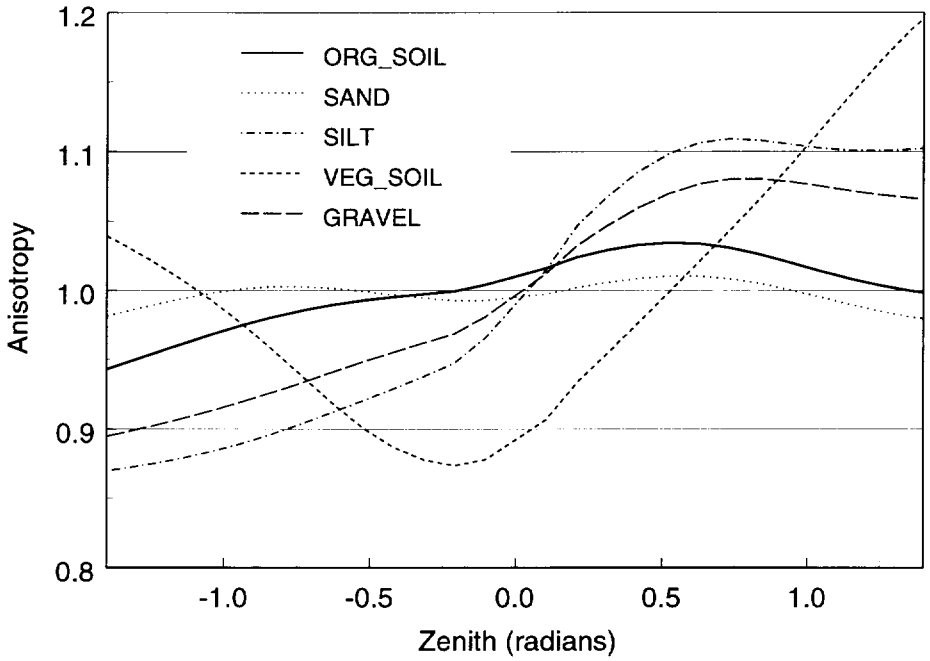

Figure 6: Anisotropy of the five materials for MODIS band 23 in the 30-degree azimuth plane. The angle of incidence is 32 degrees. Positive zenith angles represent the backscatter direction.

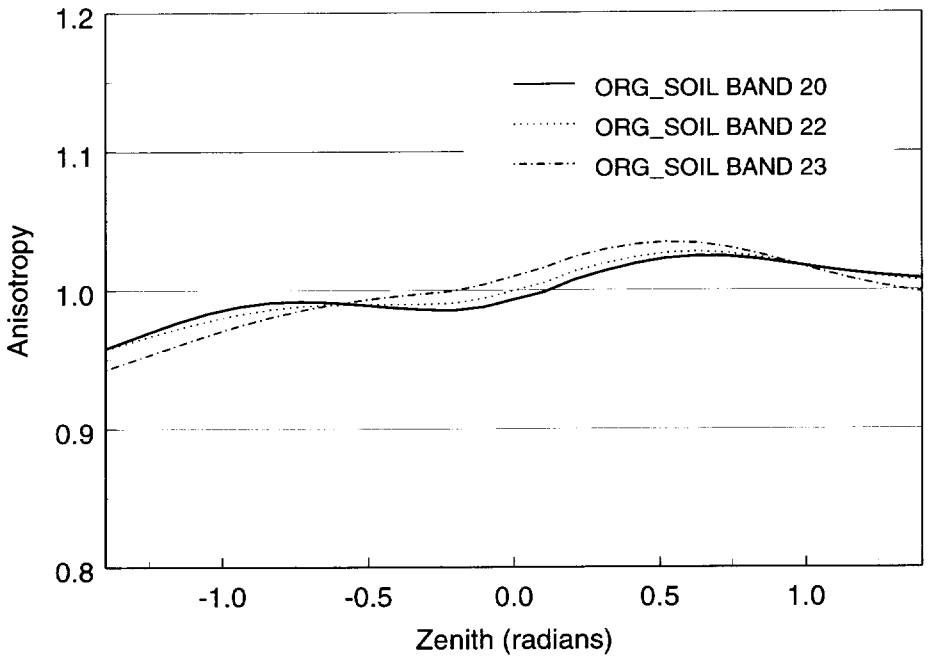

Figure 7: Anisotropy of the organic soil in each of the three MODIS bands. The geometries are the same as for Figure 6.

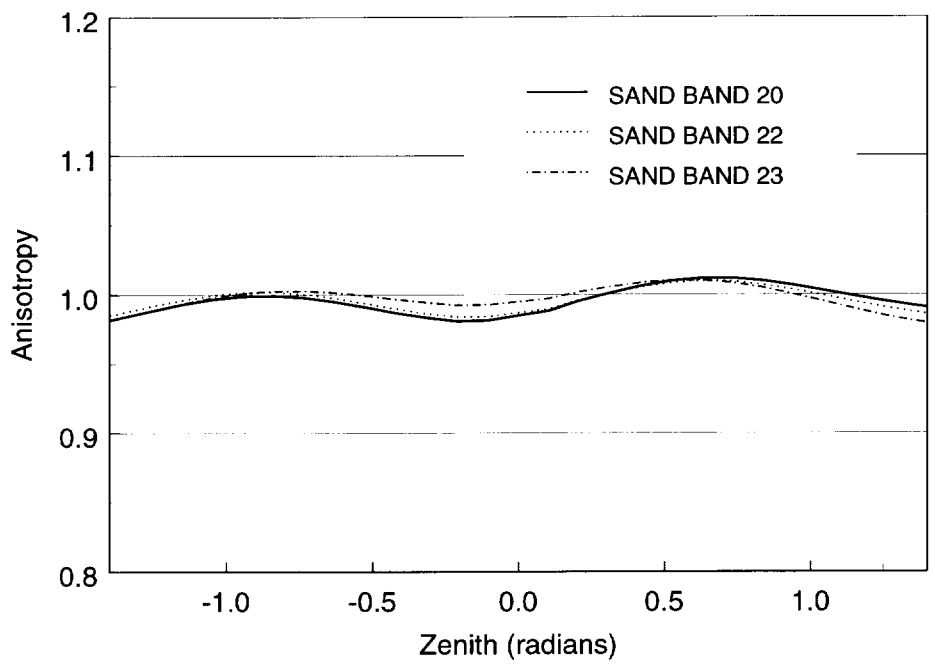

Figure 8: Anisotropy variation for sand.

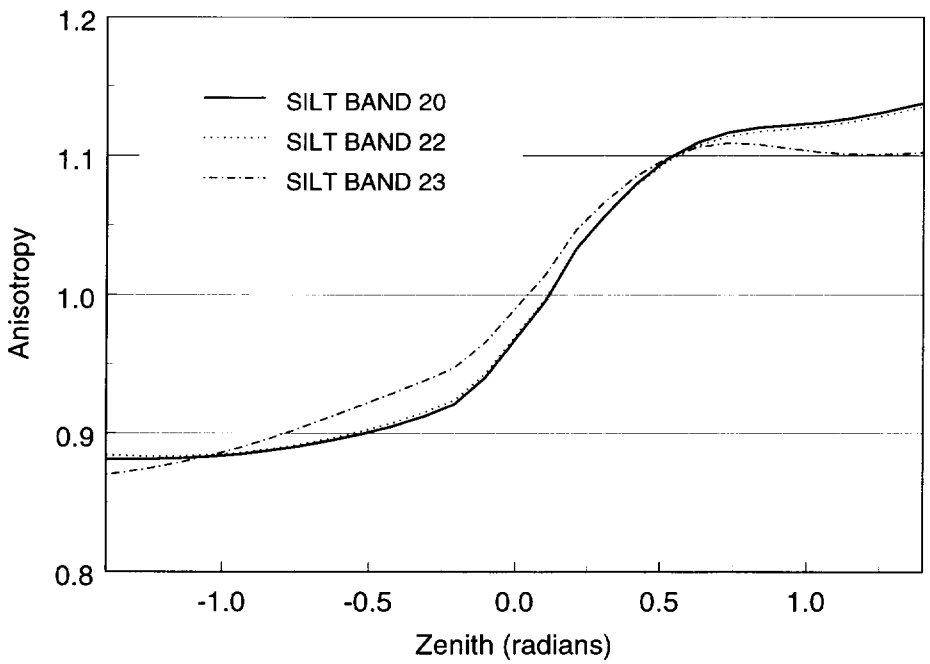

Figure 9: Anisotropy variation for silt.

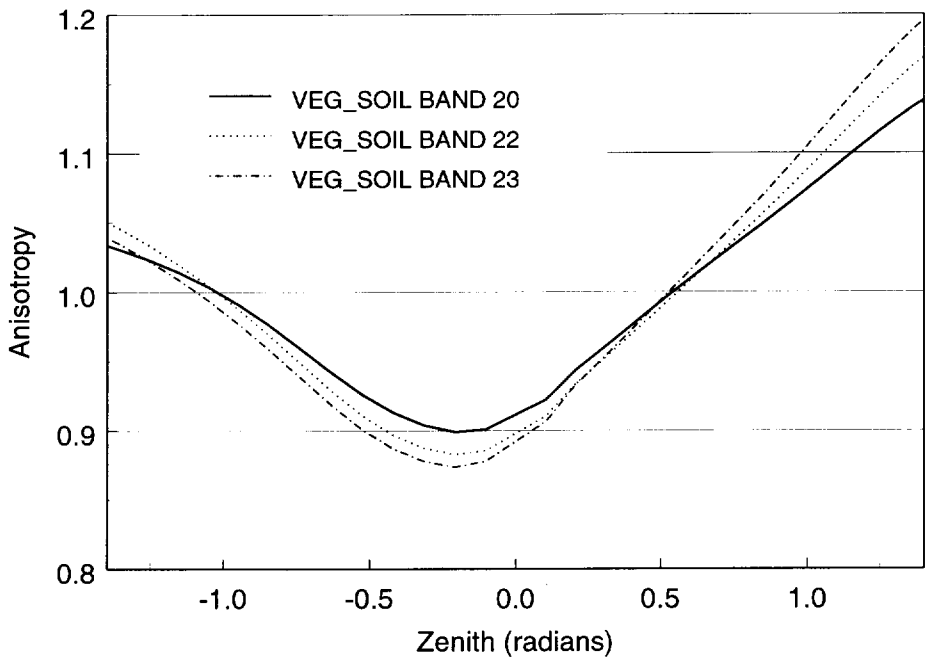

Figure 10: Anisotropy variation for the soil/vegetation mix.

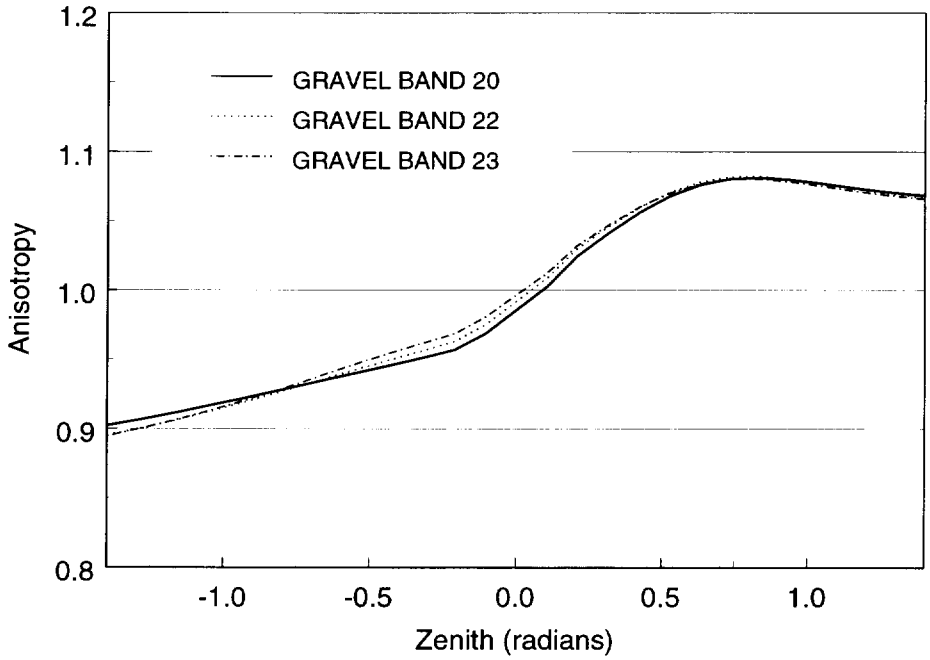

Figure 11: Anisotropy variation for gravel.